20

Human soft tissue phantom for terahertz imaging and spectroscopy

© A.S. Kucheryavenko[1], I.N. Dolganova[1], N.V. Chernomyrdin[2], A.A. Gavdush[2], D.R. Il'enkova[2], D.D. Rybnikov[2], V.M. Masalov[1], V.V. Tuchin[3,4,5], K.I. Zaytsev[2]

[1] Osipyan Institute of Solid State Physics of the Russian Academy of Sciences,
142432 Chernogolovka, Russia
[2] Prokhorov General Physics Institute of the Russian Academy of Sciences,
119991 Moscow, Russia
[3] Saratov State University,
410012 Saratov, Russia
[4] National Research Tomsk State University,
634050 Tomsk, Russia
[5] Institute of Precision Mechanics and Control, FRC „Saratov Scientific Centre of the Russian Academy of Sciences",
410028 Saratov, Russia

e-mail: ans.kucher@mail.ru

Received February 01, 2024
Revised February 20, 2024
Accepted March 05, 2024

Over the past decades, terahertz radiation has found many biomedical applications, such as marker-free diagnosis of malignant tumors, monitoring wound healing, studying brain pathologies, monitoring graft viability, etc. Most of these applications assume that soft tissues are optically homogeneous in the terahertz wavelength range, and the marker of the pathological process is the differences in the values of the complex dielectric permittivity obtained within the framework of the formalism of the effective medium theory. Meanwhile, recent advances in terahertz imaging with subwavelength spatial resolution have made it possible to detect spatial heterogeneities in the distribution of complex dielectric permittivity with dimensions comparable to the terahertz wavelength in neural, fibrous, muscle and other types of tissue. The presence of such contrasting inclusions can lead to the effects of scattering of terahertz waves at their boundaries. This raises the problem of studying the phenomena of absorption and scattering of terahertz waves in soft tissues. To solve it, it is necessary to use a phantom with previously known parameters. At the moment, there are no phantoms with scattering properties for the terahertz range. In the interests of this task, a tissue-simulating phantom was proposed in this work, which has the shape of a gelatin plate and is a highly absorbent hydration matrix into which silicon dioxide (SiO_2) microspheres are embedded with a lower refractive index and absorption coefficient, as well as subwavelength or mesoscale diameters. The terahertz images of this phantom are similar to those of a number of soft tissues, which allows its use in studies of new methods of terahertz imaging and spectroscopy.

Keywords: terahertz radiation, biological tissue phantom, terahertz imaging, subwavelength spatial resolution, Abbe diffraction limit, solid immersion effect.

DOI: 10.61011/EOS.2024.03.58752.40-24

Introduction

The application range of terahertz (THz) technologies, which includes applications in various branches of biophotonics and medicine [3–5], is currently expanding [1,2]. Of particular interest is the capacity of THz radiation to perform marker-free diagnostics of malignant and benign neoplasms [6], non-invasive monitoring of blood glucose levels [7], and quantitative evaluation of the diabetic foot syndrome [8]; establish the degree and area of traumatic injuries [9] and burn wounds [10]; monitor graft viability [11], scar healing [12], and transdermal delivery of drugs [13]; and examine the degree of hydration of the cornea and sclera in ophthalmology [14,15] and brain pathology in neurodiagnostics and neurosurgery [16]. In addition, intense THz pulses have been demonstrated to exert a nonthermal influence on tissues; these effects may be used in therapy [17].

Most of the mentioned applications rely on the assumption that tissues are optically isotropic and homogeneous in the THz range [6,17]. The THz response of soft tissues is often characterized with the use of various relaxation models of complex permittivity within the effective medium theory (EMT) formalism [18]. The energy of hydrogen bonds, which are fundamental for all biological systems, is comparable to the energy of a THz quantum. Therefore, tissue water is the factor governing the THz response of soft tissues, since the absorption of radiation by water is significant and the concentration of water in such tissues is high [19]. Just as in water and aqueous solutions, the THz complex permittivity of biological tissues is commonly characterized by a superposition of two or more relaxation-like terms with different relaxation times [20]. The Debye

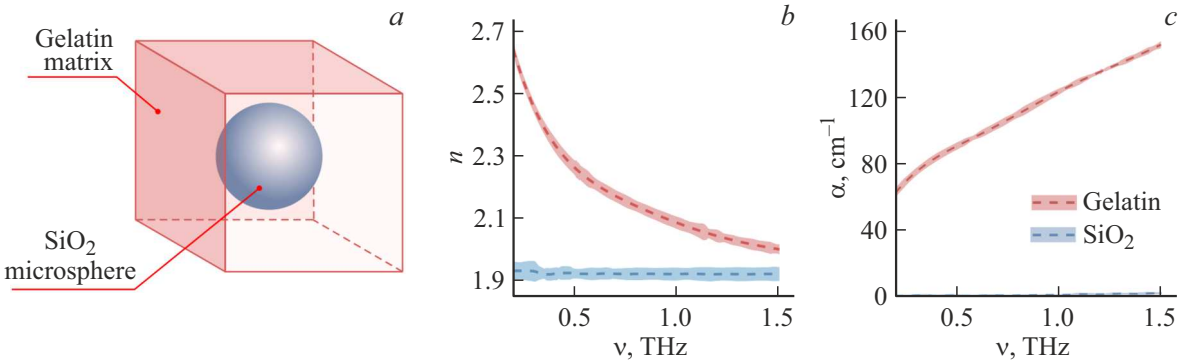

Figure 1. (*a*) A schematic of the phantom, (*b*) THz refraction index, and (*c*) amplitude absorption coefficient for pure gelatin and amorphous SiO_2 determined by THz pulse spectroscopy (from [47,48]).

model [21] is the one used most widely here, while the Cole–Cole [22,23], Cole–Davidson [24], and Havriliak–Negami [25] models or an overdamped Lorentz oscillator [26] are rarely used.

The EMT coupled with linear spectral decomposition [27], the Bruggeman model [28], or other approaches provides reliable estimates of the water content and state in tissues based on THz dielectric spectra, allowing one to use free and bound molecules of water as the main endogenous marker sensitive to various vital processes in living tissues and cells [18]. This enables the use of THz spectroscopy and imaging in medical diagnostics.

The study of propagation of THz waves in tissues, development of theoretical models, and testing of new instrumental approaches with the use of human biological tissues or model animals are challenging tasks for a number of reasons. Since contrasts between healthy and pathological tissues in THz spectra and images are induced primarily by differences in tissue water content, tissue studies should be performed immediately (or as soon as practically possible) after excision to minimize dehydration caused by interactions with the environment and degenerative changes due to cessation of blood flow. In addition, when working with tissues, one usually has to deal with high variability in permittivity of the medium and in size, shape, and permittivity of tissue inclusions, which may act as scatterers. These parameters may vary from one human or animal body to another and even within an individual sample. At the same time, a comprehensive study of the propagation of THz waves in tissues should include a very large number of samples with well-known properties that remain unchanged during the experiment and reproducible from one experiment to the next.

In biophotonics, these issues are often addressed through the use of phantoms (i.e., artificially created objects that allow one to simulate the properties of tissues of the human body) in the terahertz range and in other spectral ranges [18]. Specifically, the layered structure of the skin, microvasculature, and frequency-dependent interference effects in THz pulsed imaging may be studied using the TX151 [29] gelling agent, and two-component (consisting of water emulsions and lipids or water and gelatin) or three-component (consisting mainly of oil, gelatin, and water) phantoms were proposed to be used as models of breast tissue [30]. Contact lenses have been examined as potential corneal phantoms [31]. Various phantoms based on aqueous solutions, suspensions, and mixtures of strongly subwavelength particles or powders with particle sizes $\ll 0.1\lambda$, hydrogels, and other substances [18,29,30,32–36] have also been developed recently for the THz range. All the above phantoms are homogeneous in the THz wavelength range and are designed for verification of research methods based on EMT (analysis of sample composition, tissue water content and state, etc.), but cannot be used to model optically inhomogeneous media in the THz range.

Meanwhile, more and more studies reporting on inhomogeneities in tissues (human, animal, or even plant) comparable in size to THz wavelengths ($\sim\lambda$) are being published. For example, various high-resolution THz microscopy techniques were used in [37–39] to visualize subwavelength ($<\lambda$) or mesoscale ($\sim\lambda$) structural elements in tissues (down to an individual cell). Heterogeneities of various tissues of the mammary gland, tongue, pericardium, and brain (of humans or model animals) [40–42] were detected with an original solid immersion (SI) microscope with a resolution of 0.15λ. This microscope was also used to quantify the distribution of THz optical properties and water content in the surface layers of tissues. Scanning point terahertz source microscopy was used in [39] to analyze the heterogeneity of unstained comedo ductal carcinoma. With the advent of innovative THz imaging methods, the number of observed sub-wavelength and mesoscale tissue inhomogeneities grows annually [43–45]; however, studies of the mechanism of scattering of THz waves off observed inhomogeneities and its effect on images and spectral characteristics of samples are still incipient and require the development of additional methods and experimental techniques.

Considering all these issues, it was proposed to design and fabricate a phantom that simulates soft tissue. It should

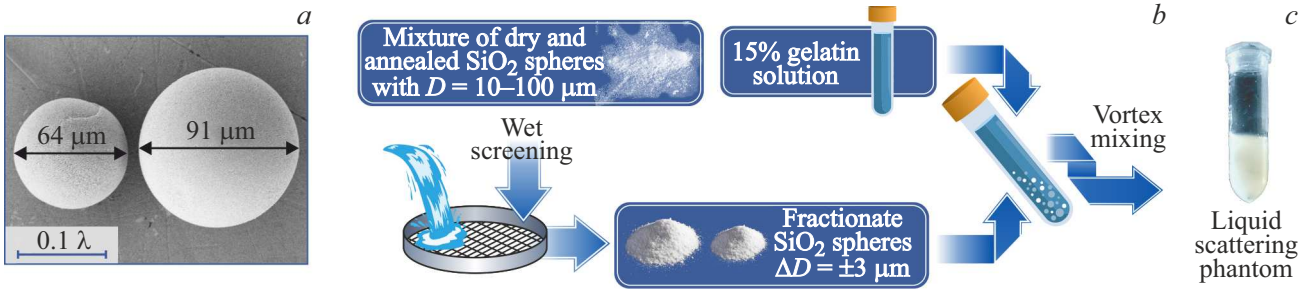

Figure 2. (*a*) Scanning electron microscopy of SiO_2 microspheres with diameters $d = 63$ and $93\,\mu$m, respectively; $\lambda = 500\,\mu$m. (*b*) A schematic of the process of fabrication of a scattering phantom based on a gelatin plate and SiO_2 microspheres. (*c*) Photographic image of a liquid phantom with volume fraction $f_v = 0.058$ of microspheres.

have a reproducible response at THz frequencies and be easy to manufacture even in large quantities. The absorption and scattering of THz radiation are modeled in it is through the inclusion of particles with varying values of diameter and volume fraction. The phantom has the form of a gelatin plate (hydrated collagen matrix, matrix medium) with high absorption in the THz range into which SiO_2 microspheres are embedded. These spheres act as sub-wavelength and mesoscale scatterers with much lower refraction indices and attenuation coefficients (compared to the matrix medium). The maximum examined diameter is close to the depth of penetration of THz waves into soft tissues and the diffraction resolution limit of THz optics. This phantom was studied by optical microscopy and high-resolution THz SI microscopy. Optical microscopy revealed the homogeneity of distribution of microspheres throughout the volume of the phantom and a small number of air bubbles in the suspension and verified that the phantom corresponds to its theoretical model. SI microscopy data demonstrated that the phantom is heterogeneous in nature (with changes in the nature of visualized inhomogeneities depending on the volume fraction and diameter of inclusions), suggesting that it is suitable for simulating a number of tissues in the THz range.

Design and fabrication of a soft tissue phantom

Connective tissue with isolated inclusions of adipose tissue cells was chosen as the soft tissue type to be modeled, since it is the simplest in terms of simulation and subsequent theoretical analysis. Terahertz spectra of adipose and connective tissues [46] demonstrate that adipose tissue is non-absorbing compared to the connective one. The model then takes the form of a single spherical non-absorbing scatterer $10-100\,\mu$m in diameter (this corresponds to the approximate size of a mature adipose tissue cell) surrounded by an absorbing matrix, which is homogeneous in the THz range and is similar in its THz dielectric properties to connective tissue.

Silicon dioxide (SiO_2) microspheres were chosen to be used as spherical scatterers for the phantom. The THz optical properties of this material are presented in Fig. 1. These spheres were fabricated in three stages. The first stage was the synthesis of colloidal SiO_2 nanoparticles $\simeq 280$ nm in diameter by a multistage method [49] that combines two known sequential methods of tetraethoxysilane hydrolysis: heterogeneous hydrolysis catalyzed by L-arginine [50] and the traditional Stöber approach [51]. The diameter deviation of SiO_2 nanoparticles was less than 3%. SiO_2 microspheres in the form of opal-like nanoparticle aggregates with a density of $\simeq 1.2\,$g/cm^3 [52] and a diameter spread of $10-110\,\mu$m were then obtained by spray drying from a concentrated suspension of SiO_2 nanoparticles. The final stage involved annealing of the microspheres performed at a temperature of $\simeq 1050^\circ$C for 24 h to remove residual water and organic components and increase their strength and density. Thus, the density of microspheres increased to $\rho_{SiO_2} \simeq 2.0\,$g/cm^3 [53], while their diameter decreased slightly as a result of collapse of nanopores inside SiO_2 nanoparticles and vanishing of pores between them. Nanoparticles could still have a residual internal porosity of several percent with a certain number of closed pores, but this number is so small that the influence of residual porosity on the THz response of microspheres could be excluded from further consideration. The obtained SiO_2 microspheres with diameters $d = 63 \pm 3$ and $93 \pm 3\,\mu$m are shown in Fig. 2, *a*.

A 15% (by weight) aqueous solution of gelatin was chosen as a fibrous absorbing matrix for the phantom. The THz optical properties of this solution are also presented in Fig. 1. The absorption coefficient of the matrix is several times higher than the absorption coefficient of spherical scatterers (this corresponds to the model conditions), but exceeds slightly the absorption coefficient of connective tissue [46].

The diagram of the process of fabrication of the phantom is shown in Fig. 2, *b*. Microspheres were first subjected to wet dispersion through a series of sieves with different hole diameters. These microspheres grouped into fractions with a diameter deviation of $\pm 3\,\mu$m within a fraction were

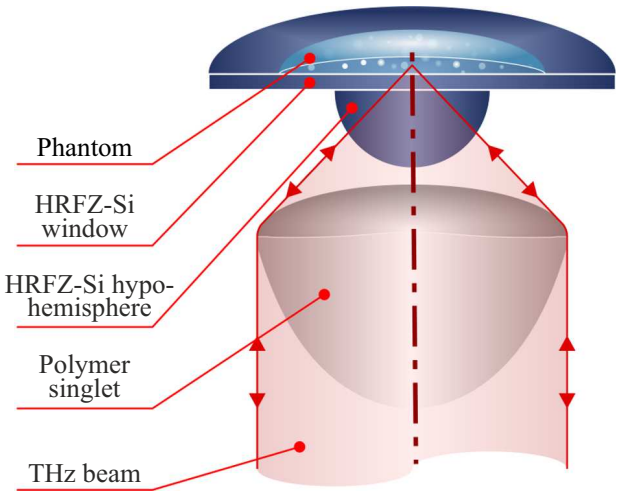

Figure 3. A schematic of an SI lens made of HRFZ-Si operating in the reflection mode in a microscope with a resolution of 0.15λ and a frequency of 0.6 THz on top of which a phantom is placed.

then introduced into a 15% aqueous solution of gelatin preheated to a temperature of 35–40°C. In mixing, we used the relation between the mass of microparticles and mass f_m of the resulting suspension, which is related to volume fraction f_v of microspheres in the following way:

$$f_v = \left(1 + \frac{1 - f_m}{f_m}\frac{\rho_{SiO_2}}{\rho_{gelatin}}\right)^{-1}, \qquad (1)$$

where $\rho_{SiO_2} \simeq 2.0\,g/cm^3$ and $\rho_{gelatin} \simeq 1.1\,g/cm^3$ are the densities of SiO_2 microspheres and pure gelatin. The suspension was sealed against the influence of air, subjected to vortex mixing without foaming, and cooled. When cooled, the viscosity of the gelatin solution increases, preventing the rapid settling of microspheres. Before the hardening of gelatin, the suspension was transferred to a pre-cooled object window of a THz-SI microscope (Fig. 3) with a pipette. There, the suspension solidified quickly and formed a phantom. Volume fraction f_v of microspheres in this phantom may be as high as 25%. Higher volume fractions may also be obtained, but this requires additional control of temperature and viscosity of the suspension.

The homogeneity of microparticle distribution throughout the volume of the phantom was checked additionally by optical microscopy. The obtained results are presented in Figs. 4, *a, c, e, g*. The fabricated phantom simulates soft tissue formed by a highly absorbent medium with embedded spherical scatterers with a much lower refraction index and losses in the THz range, is easy to manufacture, and offers fine reproducibility of properties (e.g., uniformity in diameter and type of scatterers, as well as uniformity of their distribution throughout the volume of the medium).

THz SI microscopy studies of scattering phantoms

A proprietary SI microscope operating in reflection with a resolution of 0.15λ was used to examine the distribution of microspheres inside the phantom and compare THz images of the phantom with observed inhomogeneities of freshly excised tissues. The design and operating principles of this microscope were discussed in detail in [28,40,54–56]. A backward wave oscillator [57] was used as a source of continuous radiation at a frequency of 0.6 THz (or a wavelength of $\lambda = 500\,\mu m$), and a Golay cell (opto-acoustic detector) was the receiver [58].

Figure 3 shows the schematic of the key component of the microscope: SI lens. It consists of three main elements:

- wide-aperture aspherical lens made of high-density polyethylene (HDPE); the native resolution of this lens is 0.55λ [59];
- hypo-hemisphere made of high-resistivity float-zone silicon (HRFZ-Si) and positioned in front of the focal plane in such a way that the spherical surface is concentric to the converging wavefront and the flat surface is perpendicular to the optical axis;
- plane-parallel window made of HRFZ-Si that is in contact with the hypo-hemisphere, forming a single optical element.

The hypo-hemisphere with the plane-parallel window serve as a resolution amplifier for the aspherical lens, increasing the overall resolution of the system to 0.15λ [56]. The aspherical lens and the hypo-hemisphere are rigidly fixed, while the window is movable and mounted on a horizontal displacement mechanism. This composite design provides an opportunity to image amorphous objects and soft tissues positioned on the window by scanning them with a focused THz beam. The resulting THz image has the form of a THz field intensity distribution along the image plane. As was discussed in detail in [28], the reflection of a THz beam at the window–object interface is complex due to its wide aperture, long coherence length, and the interaction of ordinary and total internal reflection phenomena. However, the problem of quantifying the analyzed refraction index for non-planar scatterers out of close contact with the HRFZ-Si window remains a challenging one and is a target for future research [28].

In preparation for THz imaging, a slightly heated liquid suspension of SiO_2 microspheres in a gelatin solution was pipetted into the HRFZ-Si window (Fig. 2, *a*). A droplet with a thickness > 1 mm and a uniform distribution of microspheres solidified quickly, forming a phantom to be imaged on top of the window. Several tissue-simulating phantoms with different diameters and volume fractions of microspheres were prepared.

The results of optical and THz microscopy for phantoms with volume fractions of microspheres $f_v = 0.0056$ and 0.0284, which correspond to mass fractions of 1 and 5%, and diameters $d = 63$ and $93\,\mu m$, respectively, are presented in Figs. 4, *a–h*. Optical images reveal a

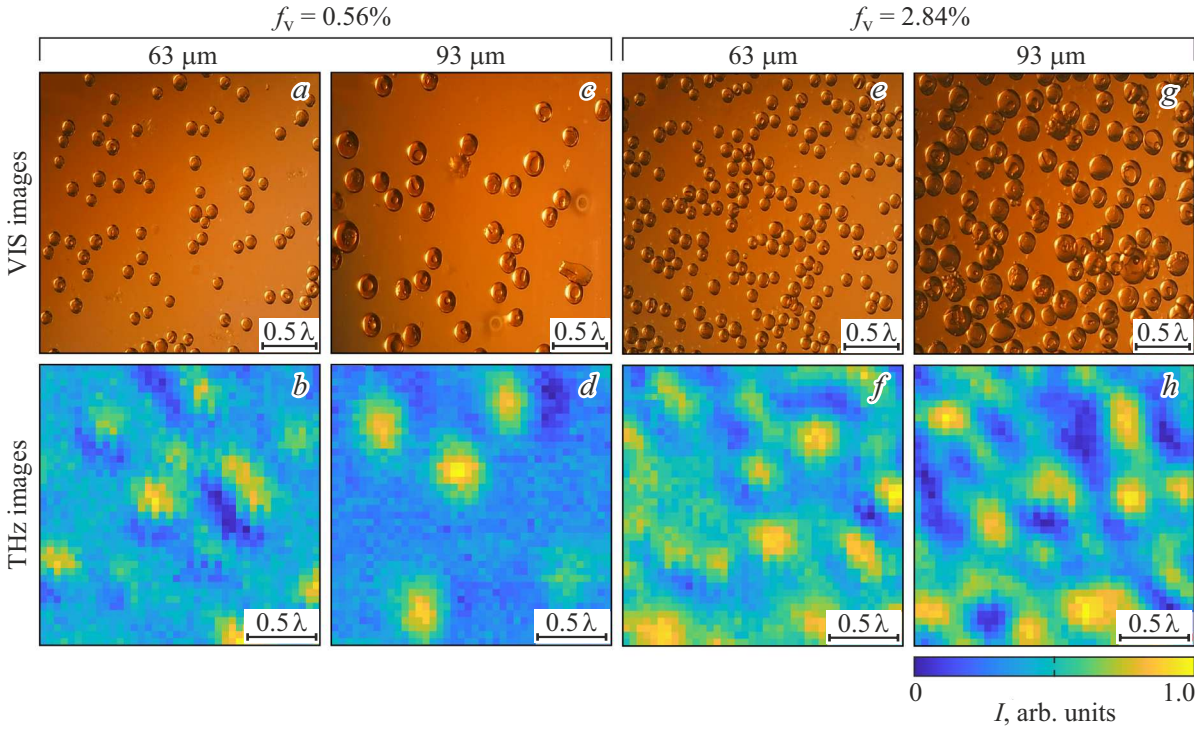

Figure 4. Terahertz SI microscopy data for tissue-simulating phantoms obtained at a frequency of 0.6 THz ($\lambda = 500\,\mu$m) with a resolution up to 0.15λ. (a, b) Optical and THz microscopic images of a phantom with particle diameter $d = 63\,\mu$m and volume fraction $f_v = 0.0056$. (c, d) Data for a phantom with particle diameter $d = 93\,\mu$m and the same volume fraction. (e, f) Optical and THz microscopic images of a phantom with particle diameter $d = 63\,\mu$m and volume fraction $f_v = 0.0284$. (g, h) Data for a phantom with particle diameter $d = 93\,\mu$m and the same volume fraction.

uniform distribution of particles throughout the volume of the phantom at the chosen volume concentrations. Air bubbles located in the bulk of the phantom or on the rough surface of microspheres are also seen, but their number is extremely small, and their contribution to changes in the THz optical properties of the phantom may thus be neglected. The reflectivity of the phantom varies in the THz imaging plane on the desired sub-wavelength scale due to the presence of SiO_2 inclusions. The scattering particles in Figs. 4, *b*, *f* are slightly smaller than the resolution of the THz microscope ($0.126\lambda < 0.15\lambda$), but changes in the intensity of the backscattered THz field caused by each microsphere are observed, and the image inhomogeneity becomes more pronounced as the concentration increases. In contrast, Fig. 4, *d* allows one to distinguish clearly individual SiO_2 microspheres of a larger diameter ($0.186\lambda > 0.15\lambda$). At a higher volume fraction (Fig. 4, *h*), individual particles are no longer visualized clearly enough due to the overlap of backscattered waves from microspheres located in the volume of the medium. One may also note that with volume fraction of microspheres $f_v = 2.84\%$, inhomogeneities created by particles with a diameter of $63\,\mu$m (Fig. 4, *f*) are somewhat smaller in size than those corresponding to microspheres with a diameter of $93\,\mu$m (Fig. 4, *h*). This provides the prerequisites for a possible solution to the inverse problem (determining the true sizes of tissue inclusions from a THz image).

The discussed phantom is especially important for advancing the technology of optical clearing of tissues in the THz range [60,61], where the scattering effects need to be analyzed thoroughly in both hydrated and dehydrated (by a hyperosmotic agent) tissue. Hyperosmotic immersion agents used to suppress the absorption of THz waves in tissues can either unmask scattering processes or reduce the dielectric contrast between the matrix medium and scatterers and, consequently, lower both the absorption of THz waves by tissue water and the scattering efficiency.

Since materials producing a fairly strong dielectric contrast (between the absorbing matrix and an individual scatterer) and allowing for a wide range of variation of the scatterer parameters were used to construct the phantom, it has the capacity to simulate various soft tissues of the body in the THz range [6,17,18] (e.g., the structure of the mammary gland with lobules and single fat cells surrounded by connective tissue [56]). In addition, mesoscale scatterers with a near-spherical shape and a lower THz refraction index and losses may form in pathologically altered tissues, e.g., in the case of accumulation of tumor cells and necrotic debris in tumors and traumatic brain injuries [9,28], accumulation of fat cells associated with the fatty liver disease [62], aggregation of beta-amyloid in nerve

tissues associated with the Alzheimer's disease [63], sperm agglutination [64], etc. However, deviations from the ideal spherical shape of a single diffuser need to be taken into account in some of these tissues.

It should be stressed that the designed phantom simulates only a limited number of soft tissues in the THz range. Tissues with a completely different kind of (potentially anisotropic) geometry, density, and packing of scatterers and other values of the dielectric contrast between scatterers and the matrix medium are perfectly conceivable. For example, to create a muscle tissue phantom, one needs to take into account the parallel alignment of muscle fibers in a bundle, which may lead to THz birefringence or parametric resonance in tissues [41,65].

In our future research, we plan to develop other tissue-simulating phantoms with a wide range of parameters and different radiation transfer modes. The ultimate goal is to adapt these approaches to characterization of the interactions of THz waves with real turbid tissues.

Conclusion

A human soft tissue phantom based on a gelatin plate and SiO_2 microparticles, which act as a highly absorbent matrix and dielectric scatterers, respectively, was proposed. The dielectric parameters of its components are similar to the parameters of adipose and connective tissues, while the variability of diameters and volume concentrations of scattering microspheres allow one to simulate a number of soft tissues and their pathologies. Optical and THz microscopy data prove that this phantom has application potential as a universal model medium for the development and testing of new experimental techniques of THz microscopy and spectroscopy.

Funding

This study was supported by the Russian Science Foundation (project No. 19-79-10212).

Conflict of interest

The authors declare that they have no conflict of interest.

References

[1] S. Lepeshov, A. Gorodetsky, A. Krasnok, E. Rafailov, P. Belov. Laser Photon Rev., **11** (1), 1600199 (2017). DOI: 10.1002/lpor.201600199

[2] H. Guerboukha, K. Nallappan, M. Skorobogatiy. Adv. Opt. Photonics, **10** (4), 843 (2018). DOI: 10.1364/AOP.10.000843

[3] X. Yang, X. Zhao, K. Yang, Y. Liu, Y. Liu, W. Fu, Y. Luo. Trends Biotechnol., **34** (10), 810 (2016). DOI: 10.1016/j.tibtech.2016.04.008

[4] H. Lindley-Hatcher, R.I. Stantchev, X. Chen, A.I. Hernandez-Serrano, J. Hardwicke, E. Pickwell-MacPherson. Appl. Phys. Lett., **118** (23), 230501 (2021). DOI: 10.1063/5.0055259

[5] Z. Yan, L.-G. Zhu, K. Meng, W. Huang, Q. Shi. Trends Biotechnol., **40** (7), 816 (2022). DOI: 10.1016/j.tibtech.2021.12.002

[6] K.I. Zaytsev, I.N. Dolganova, N. V. Chernomyrdin, G.M. Katyba, A.A. Gavdush, O.P. Cherkasova, G.A. Komandin, M.A. Shchedrina, A.N. Khodan, D.S. Ponomarev, I.V. Reshetov, V.E. Karasik, M. Skorobogatiy, V.N. Kurlov, V.V. Tuchin. J. Optics, **22** (1), 13001 (2019). DOI: 10.1088/2040-8986/ab4dc3

[7] O. Cherkasova, M. Nazarov, A. Shkurinov. Opt. Quantum Electron., **48**, 217 (2016). DOI: 10.1007/s11082-016-0490-5

[8] G.G. Hernandez-Cardoso, L.F. Amador-Medina, G. Gutierrez-Torres, E.S. Reyes-Reyes, C.A.B. Martínez, C.C. Espinoza, J.A. Cruz, I. Salas-Gutierrez, B.O. Murillo-Ortiz, E. Castro-Camus. Sci. Rep., **12**, 3110 (2022). DOI: 10.1038/s41598-022-06996-w

[9] H. Zhao, Y. Wang, L. Chen, J. Shi, K. Ma, L. Tang, D. Xu, J. Yao, H. Feng, T. Chen. J. Biomed. Opt., **23** (3), 36015 (2018). DOI: 10.1117/1.JBO.23.3.036015

[10] N. Bajwa, S. Sung, D.B. Ennis, M.C. Fishbein, B.N. Nowroozi, D. Ruan, A. Maccabi, J. Alger, M.A.St. John, W.S. Grundfest, Z.D. Taylor. IEEE Trans. Biomed. Eng., **64** (11), 2682 (2017). DOI: 10.1109/TBME.2017.2658439

[11] N. Bajwa, J. Au, R. Jarrahy, S. Sung, M.C. Fishbein, D. Riopelle, D.B. Ennis, T. Aghaloo, M.A. St.-John, W.S. Grundfest, Z.D. Taylor. Biomed. Opt. Express, **8** (1), 460 (2017). DOI: 10.1364/BOE.8.000460

[12] J. Wang, Q. Sun, R.I. Stantchev, T.-W. Chiu, A.T. Ahuja, E. Pickwell-MacPherson. Biomed. Opt. Express, **10** (7), 3584 (2019). DOI: 10.1364/BOE.10.003584

[13] X. Ding, G. Costa, A.I. Hernandez-Serrano, R.I. Stantchev, G. Nurumbetov, D.M. Haddleton, E. Pickwell-MacPherson. Biomed. Opt. Express, **14** (3), 1146 (2023). DOI: 10.1364/BOE.473097

[14] E.N. Iomdina, G.N. Goltsman, S.V. Seliverstov, A.A. Sianosyan, K.O. Teplyakova, A.A. Rusova. J. Biomed. Opt., **21** (9), 97002 (2016). DOI: 10.1117/1.JBO.21.9.097002

[15] E.N. Iomdina, S.V. Seliverstov, K.O. Teplyakova, E.V. Jani, V.V. Pozdniakova, O.N. Polyakova, G.N. Goltsman. J. Biomed. Opt., **26** (4), 43010 (2021). DOI: 10.1117/1.JBO.26.4.043010

[16] N.V. Chernomyrdin, G.R. Musina, P.V. Nikitin, I.N. Dolganova, A.S. Kucheryavenko, A.I. Alekseeva, Y. Wang, D. Xu, Q. Shi, V.V. Tuchin, K.I. Zaytsev. Opto-Electron. Advances, **6**, 220071 (2023). DOI: 10.29026/oea.2023.220071

[17] O.P. Cherkasova, D.S. Serdyukov, E.F. Nemova, A.S. Ratushnyak, A.S. Kucheryavenko, I.N. Dolganova, G. Xu, M. Skorobogatiy, I.V. Reshetov, P.S. Timashev, I.E. Spektor, K.I. Zaytsev, V.V. Tuchin. J. Biomed. Opt., **26** (9), 90902 (2021). DOI: 10.1117/1.JBO.26.9.090902

[18] O.A. Smolyanskaya, N.V. Chernomyrdin, A.A. Konovko, K.I. Zaytsev, I.A. Ozheredov, O.P. Cherkasova, M.M. Nazarov, J.-P. Guillet, S.A. Kozlov, Yu.V. Kistenev, J.-L. Coutaz, P. Mounaix, V.L. Vaks, J.-H. Son, H. Cheon, V.P. Wallace, Yu. Feldman, I. Popov, A.N. Yaroslavsky, A.P. Shkurinov, V.V. Tuchin. Prog. Quantum Electron., **62**, 1 (2018). DOI: 10.1016/j.pquantelec.2018.10.001

[19] U. Møller, D.G. Cooke, K. Tanaka, P.U. Jepsen. J. Opt. Sci. Am. B, **26** (9), A113 (2009). DOI: 10.1364/JOSAB.26.00A113

[20] I. Popov, P.B. Ishai, A. Khamzin, Y. Feldman. Phys. Chem. Chem. Phys., **18** (20), 13941 (2016). DOI: 10.1039/C6CP02195F

[21] E. Pickwell, B.E. Cole, A.J. Fitzgerald, V.P. Wallace, M. Pepper. Appl. Phys. Lett., **84** (12), 2190 (2004). DOI: 10.1063/1.1688448
[22] K.S. Cole, R.H. Cole. J. Chem. Phys., **9** (4), 341 (2004). DOI: 10.1063/1.1750906
[23] K.S. Cole, R.H. Cole. J. Chem. Phys., **10** (2), 98 (2004). DOI: 10.1063/1.1723677
[24] D.W. Davidson, R.H. Cole. J. Chem. Phys., **18** (10), 1417 (2004). DOI: 10.1063/1.1747496
[25] S. Havriliak, S. Negami. Polymer (Guildf), **8**, 161 (1967). DOI: 10.1016/0032-3861(67)90021-3
[26] A.A. Gavdush, N.V. Chernomyrdin, G.A. Komandin, I.N. Dolganova, P.V. Nikitin, G.R. Musina, G.M. Katyba, A.S. Kucheryavenko, I.V. Reshetov, A.A. Potapov, V.V. Tuchin, K.I. Zaytsev. Biomed. Opt. Express, **12** (1), 69 (2021). DOI: 10.1364/BOE.411025
[27] S. Yamaguchi, Y. Fukushi, O. Kubota, T. Itsuji, T. Ouchi, S. Yamamoto. Phys. Med. Biol., **61** (18), 6808 (2016). DOI: 10.1088/0031-9155/61/18/6808
[28] N.V. Chernomyrdin, M. Skorobogatiy, A.A. Gavdush, G.R. Musina, G.M. Katyba, G.A. Komandin, A.M. Khorokhorov, I.E. Spektor, V.V. Tuchin, K.I. Zaytsev. Optica, **8** (11), 1471 (2021). DOI: 10.1364/OPTICA.439286
[29] G.C. Walker, E. Berry, S.W. Smye, D.S. Brettle. Phys. Med. Biol., **49** (21), N363 (2004). DOI: 10.1088/0031-9155/49/21/N01
[30] B.C.Q. Truong, A.J. Fitzgerald, S. Fan, V.P. Wallace, V.I.P.W. Allace, B.C.Q. Truong, A.J. Fitzgerald, S. Fan, V.P. Wallace. Biomed. Opt. Express, **9** (3), 1334 (2018). DOI: 10.1364/BOE.9.001334
[31] A. Chen, O.B. Osman, Z.B. Harris, A. Abazri, R. Honkanen, M.H. Arbab. Biomed. Opt. Express, **11** (3), 1284 (2020). DOI: 10.1364/BOE.382826
[32] G.C. Walker, E. Berry, S.W. Smye, N.N. Zinov'ev, A.J. Fitzgerald, R.E. Miles, M. Chamberlain, M.A. Smith. Phys. Med. Biol., **49** (10), 1853 (2004). DOI: 10.1088/0031-9155/49/10/002
[33] G.G. Hernandez-Cardoso, A.K. Singh, E. Castro-Camus. Appl. Opt., **59** (13), D6 (2020). DOI: 10.1364/AO.382383
[34] A. Tamminen, M. Baggio, I. Nefedova, Q. Sun, J. Anttila, J. Ala-Laurinaho, E.R. Brown, V.P. Wallace, E. Pickwell-MacPherson, T. Maloney, M. Salkola, S.X. Deng, Z.D. Taylor. IEEE Trans. Terahertz Sci. Technol., **11** (5), 538 (2021). DOI: 10.1109/TTHZ.2021.3088273
[35] A. Tamminen, M. Baggio, I.I. Nefedova, Q. Sun, S.A. Presnyakov, J. Ala-Laurinaho, E.R. Brown, V.P. Wallace, E. Pickwell-MacPherson, T. Maloney, N.P. Kravchenko, M. Salkola, S.X. Deng, Z.D. Taylor. IEEE Trans. Terahertz Sci. Technol., **11** (6), 647 (2021). DOI: 10.1109/TTHZ.2021.3099058
[36] A.A. Bakulina, G.R. Musina, A.A. Gavdush, Y.M. Efremov, G.A. Komandin, M. Vosough, A.I. Shpichka, K.I. Zaytsev, P.S. Timashev. Soft Matter., **19** (13), 2430 (2023). DOI: 10.1039/D2SM01504H
[37] K. Okada, K. Serita, Q. Cassar, H. Murakami, G. MacGrogan, J.-P. Guillet, P. Mounaix, M. Tonouchi. J. Phys.: Photonics, **2** (4), 44008 (2020). DOI: 10.1088/2515-7647/abbcda
[38] Z. Li, S. Yan, Z. Zang, G. Geng, Z. Yang, J. Li, L. Wang, C. Yao, H.-L. Cui, C. Chang, H. Wang. Cell Prolif., **53** (4), e12788 (2020). DOI: 10.1111/cpr.12788
[39] K. Okada, Q. Cassar, H. Murakami, G. MacGrogan, J.-P. Guillet, P. Mounaix, M. Tonouchi, K. Serita. Optics Continuum, **1** (3), 527 (2022). DOI: 10.1364/OPTCON.448444
[40] A.S. Kucheryavenko, N.V. Chernomyrdin, A.A. Gavdush, A.I. Alekseeva, P.V. Nikitin, I.N. Dolganova, P.A. Karalkin, A.S. Khalansky, I.E. Spektor, M. Skorobogatiy, V.V. Tuchin, K.I. Zaytsev. Biomed. Opt. Express, **12** (8), 5272 (2021). DOI: 10.1364/BOE.432758
[41] N.V. Chernomyrdin, D.R. Ilenkova, V.A. Zhelnov, A.I. Alekseeva, A.A. Gavdush, G.R. Musina, P.V. Nikitin, A.S. Kucheryavenko, I.N. Dolganova, I.E. Spektor, V.V. Tuchin, K.I. Zaytsev. Sci. Rep., **13**, 16596 (2023). DOI: 10.1038/s41598-023-43857-6
[42] N.V. Chernomyrdin, M. Skorobogatiy, D.S. Ponomarev, V.V. Bukin, V.V. Tuchin, K.I. Zaytsev. Appl. Phys. Lett., **120** (11), 110501 (2022). DOI: 10.1063/5.0085906
[43] F. Blanchard, A. Doi, T. Tanaka, H. Hirori, H. Tanaka, Y. Kadoya, K. Tanaka. Opt. Express, **19** (9), 8277 (2011). DOI: 10.1364/OE.19.008277
[44] R.I. Stantchev, B. Sun, S.M. Hornett, P.A. Hobson, G.M. Gibson, M.J. Padgett, E. Hendry. Sci. Adv., **2** (6), e1600190 (2016). DOI: 10.1126/sciadv.1600190
[45] L. Olivieri, L. Peters, V. Cecconi, A. Cutrona, M. Rowley, J. Gongora, A. Pasquazi, M. Peccianti. ACS Photonics, **10** (6), 1726 (2023). DOI: 10.1021/acsphotonics.2c01727
[46] P.C. Ashworth, E. Pickwell-MacPherson, E. Provenzano, S.E. Pinder, A.D. Purushotham, M. Pepper, V.P. Wallace. Opt. Express, **17** (15), 12444 (2009). DOI: 10.1364/OE.17.012444
[47] V.E. Ulitko, A.K. Zotov, A.A. Gavdush, G.M. Katyba, G.A. Komandin, I.E. Spektor, I.M. Shmytko, G.A. Emelchenko, I.N. Dolganova, M. Skorobogatiy, V.N. Kurlov, V.M. Masalov, K.I. Zaytsev. Opt. Mater. Express, **10** (9), 2100 (2020). DOI: 10.1364/OME.402185
[48] A.S. Kucheryavenko, I.N. Dolganova, A.A. Zhokhov, V.M. Masalov, G.R. Musina, V.V. Tuchin, N.V. Chernomyrdin, A.A. Gavdush, D.R. Il'enkova, S.V. Garnov, K.I. Zaytsev. Phys. Rev. Appl., **20** (5), 054050 (2023). DOI: 10.1103/PhysRevApplied.20.054050
[49] V.M. Masalov, N.S. Sukhinina, G.A. Emelchenko. Phys. Solid State, **53**, 1135 (2011). DOI: 10.1134/S1063783411060229
[50] K.D. Hartlen, A.P.T. Athanasopoulos, V. Kitaev. Langmuir, **24**, 1714 (2008). DOI: 10.1021/la7025285
[51] W. Stöber, A. Fink, E. Bohn. J. Colloid Interface Sci., **26** (1), 62 (1968). DOI: 10.1016/0021-9797(68)90272-5
[52] A.A. Zhokhov, V.M. Masalov, N.S. Sukhinina, D.V. Matveev, P.V. Dolganov, V.K. Dolganov, G.A. Emelchenko. Opt. Mater (Amst), **49**, 208 (2015). DOI: 10.1016/j.optmat.2015.09.019
[53] E.N. Samarov, A.D. Mokrushin, V.M. Masalov, G.E. Abrosimova, G.A. Emel'chenko. Phys. Solid State, **48**, 1280 (2006). DOI: 10.1134/S1063783406070109
[54] N.V. Chernomyrdin, A.S. Kucheryavenko, E.N. Rimskaya, I.N. Dolganova, V.A. Zhelnov, P.A. Karalkin, A.A. Gryadunova, I.V. Reshetov, D.V. Lavrukhin, D.S. Ponomarev, V.E. Karasik, K.I. Zaytsev. Opt. Spectrosc., **126** (5), 560 (2019). DOI: 10.1134/S0030400X19050059
[55] G.R. Musina, N.V. Chernomyrdin, E.R. Gafarova, A.A. Gavdush, A.J. Shpichka, G.A. Komandin, V.B. Anzin, E.A. Grebenik, M.V. Kravchik, E.V. Istranova, I.N. Dolganova, K.I. Zaytsev, P.S. Timashev. Biomed. Opt. Express, **12** (9), 5368 (2021). DOI: 10.1364/BOE.433216

[56] N.V. Chernomyrdin, A.S. Kucheryavenko, G.S. Kolontaeva, G.M. Katyba, I.N. Dolganova, P.A. Karalkin, D.S. Ponomarev, V.N. Kurlov, I.V. Reshetov, M. Skorobogatiy, V.V. Tuchin, K.I. Zaytsev. Appl. Phys. Lett., **113** (11), 111102 (2018). DOI: 10.1063/1.5045480
[57] G.A. Komandin, S.V. Chuchupal, S.P. Lebedev, Y.G. Goncharov, A.F. Korolev, O.E. Porodinkov, I.E. Spektor, A.A. Volkov. IEEE Trans. Terahertz Sci. Technol., **3** (4), 440 (2013). DOI: 10.1109/TTHZ.2013.2255914
[58] M.J.E. Golay. Rev. Sci. Instruments, **18** (5), 347 (2004). DOI: 10.1063/1.1740948
[59] N.V. Chernomyrdin, M.E. Frolov, S.P. Lebedev, I.V. Reshetov, I.E. Spektor, V.L. Tolstoguzov, V.E. Karasik, A.M. Khorokhorov, K.I. Koshelev, A.O. Schadko, S.O. Yurchenko, K.I. Zaytsev. Rev. Sci. Instruments, **88** (1), 14703 (2017). DOI: 10.1063/1.4973764
[60] G.R. Musina, I.N. Dolganova, N.V. Chernomyrdin, A.A. Gavdush, V.E. Ulitko, O.P. Cherkasova, D.K. Tuchina, P.V. Nikitin, A.I. Alekseeva, N.V. Bal, G.A. Komandin, V.N. Kurlov, V.V. Tuchin, K.I. Zaytsev. J. Biophotonics, **13** (12), e202000297 (2020). DOI: 10.1002/jbio.202000297
[61] Handbook of Tissue Optical Clearing: New Prospects in Optical Imaging, ed. by V.V. Tuchin, D. Zhu, E.A. Genina (CRC Press, Boca Raton, Florida, USA, 2022). DOI: 10.1201/9781003025252
[62] Y.-Y. Chen, M.M. Yeh. J. Formosan Medical Association, **120** (1, Part 1), 68 (2021). DOI: 10.1016/j.jfma.2020.07.006
[63] V. Lau, L. Ramer, M.E. Tremblay. Nat. Commun., **14**, 1670 (2023). DOI: 10.1038/s41467-023-37304-3
[64] G. Chen, B. Zheng. Reproductive Biology & Endocrinology, **19**, 38 (2021). DOI: 10.1186/s12958-021-00724-1
[65] X. Chen, Q. Sun, J. Wang, H. Lindley-Hatcher, E. Pickwell-MacPherson. Adv. Photonics Res., **2** (1), 2000024 (2021). DOI: 10.1002/adpr.202000024

Translated by D.Safin